REVISTA PERSPECTIVAS

VOL. 8, N°2 / JULIO - DICIEMBRE 2026 / e-ISSN: 266-6688

https://doi.org/10.47187/perspectivas.8.2.246

# Radiation phase control system for a WIFI and BLUETOOTH antenna array using phase shifters

## Sistema de control de fase de radiación para un conjunto de antenas WIFI y BLUETOOTH mediante desplazadores de fase


| | |
|---|---|
| María Díaz [1] | mariac.diaz@espoch.edu.ec |
| Ana Ortega [2] | ana.ortegau6@espoch.edu.ec |
| Dayana Pilco [3] | dayana.pilco@espoch.edu.ec |
| José Samaniego [4] | enrique.samaniego@espoch.edu.ec |
| Ronny Toctaquiza [5] | ronny.toctaquiza@espoch.edu.ec |

[1] Escuela Superior Politécnica de Chimborazo, Riobamba, Ecuador



## RESUMEN

Este artículo presenta un sistema para controlar el ángulo de sonido y cambiar rápidamente los patrones de radiación de antenas WiFi y Bluetooth mediante la modificación del desfase en un conjunto de antenas de parche. El sistema incorpora un proceso de desfase para lograr la formación de haz, lo que mejora la intensidad de la señal en las ubicaciones deseadas y reduce el ruido en áreas no deseadas. Esto implica el diseño de antenas de parche con mediciones precisas, la instalación de una unidad de control para ajustar el desfase y la prueba de su funcionamiento en entornos reales y simulados. Las mediciones se realizaron en un patrón circular, cubriendo un área de 180 grados con 30 puntos, a intervalos de 6 grados, en una cámara anecoica. Se utilizó un voltaje de 3 V para determinar el desfase entre mediciones sin desfasador. Los resultados mostraron que sin desfasador, se encontró un valor mínimo de -25,25 dB, mientras que, con los diferentes voltajes, se obtuvo un valor de -25,29 dB a 3 V, lo que indica un desfase aproximado de 12 grados en comparación con las mediciones sin desfasador. Los datos muestran cambios significativos en la cobertura de la señal, el consumo de energía y una mejora en el rendimiento del sistema. Los hallazgos resaltan el potencial de este enfoque para su uso en hogares inteligentes, dispositivos IoT y otros sistemas de comunicación inalámbrica que requieren patrones de radiación flexibles.



**Palabras Clave:** Microrred (MG), Costo de energía (COE), Red eléctrica, HOMER Pro, Optimización energética.



## ABSTRACT

This article presents a system for controlling the angle of sound and rapidly changing the radiation patterns of WiFi and Bluetooth antennas by modifying the phase shift in a patch antenna array. The system incorporates a phase shifting process to achieve beamforming, which improves signal strength in desired locations and reduces noise in undesired areas. This involves designing patch antennas with precise measurements, installing a control unit to adjust the phase shift, and testing their operation in both real and simulated environments. Measurements were made in a circular pattern, covering a 180- degree area with 30 points, at 6-degree intervals, in an anechoic chamber. A voltage of 3 V was used to determine the phase shift between measurements without a phase shifter. The results showed that without a phase shifter, a minimum value of -25.25 dB was found, while with the different voltages, a value of -25.29 dB was obtained at 3 V, indicating an approximate phase shift of 12 degrees compared to measurements without a phase shifter. The data show significant changes in signal coverage, power utilization, and an improvement in system performance. The findings highlight the potential of this approach for use in smart homes, IoT devices, and other wireless communication systems that require flexible radiation patterns.



**Keywords:** Adaptive radiation patterns, Patch antenna beamforming, Phase shift control, Wireless signal coverage, IoT and smart home communications.

**Fecha de Recepción:** 02 Julio 2025 · **Fecha de Aceptación:** 14 Mayo 2026 · **Fecha de Publicación:** 30 Julio 2026

## I. Introduction

The increasing use of wireless communication systems has made technologies such as WiFi and Bluetooth essential elements for modern applications, ranging from IoT devices to smart home networks [1]. At the core of these systems, antennas play a critical role in determining signal coverage, efficiency, and overall system performance [2]. Patch antennas have become a preferred solution due to their compact size, ease of fabrication, and excellent performance at high frequencies [3].

The main problem with WIFI and BLUETOOTH systems is that they are manufactured to emit signals in all directions. These are omnidirectional antennas, which causes power loss by radiating energy in undesired directions [4], generate interfaces with other devices in the same band and lack directional control of the radiation pattern, limiting efficiency and range [5]. For this reason, the implementation of a phase shifter in systems with patch antenna arrays allows the radiation pattern to be modified to direct the signal in a specific direction, improving quality and efficiency [6].

The integration of phase-shifting mechanisms into antenna arrays enables advanced beamforming capabilities. By controlling the phase of signals at individual elements of an antenna array, it is possible to dynamically steer the beam in desired directions and suppress interference in undesired areas. This approach significantly improves spatial coverage and spectral efficiency of wireless networks [7] [8].

Omnidirectional antennas, common in routers and IoT devices, offer wide coverage but with lower gain, while patch antennas, with a low profile and directional pattern, are ideal for WiFi systems (2.4 GHz and 5 GHz) in our case in 2.4GHz and Bluetooth, especially in compact devices such as wearables and advanced routers with beamforming. This work seeks to design and implement a dynamic phase control system to modify in real time the radiation patterns of patch antennas, using phase shifters based on varactors or MEMS for reactive control and digital methods with FPGAs for greater precision, thus optimizing the signal performance [9].

## II. Methodology

### A. System architecture

The system consists of four main interconnected modules: signal generation, dividers, phase shifters and patch antennas. Each module has a specific purpose in the design and control of the system radiation pattern as shown in Fig. 1.

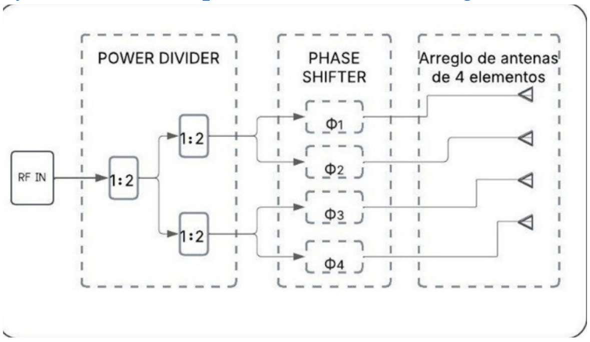


**Fig. 1.** *Phase control system diagram*

The function of each component is detailed below:

1. Signal generation: generate the carrier signal at the 2.4GHz operating frequency for WIFI and Bluetooth. For its implementation, a high-precision signal generator capable of maintaining stability in frequency and amplitude is used.

2. Divisors: three 1 to 2 dividers are used in an electrical circuit designed to divide an input voltage into two proportional output voltages, but with a 1:2 ratio. This means that the output signal has a voltage that is half the input voltage in one case, or double in another, depending on the configuration of the divider. It is a concept commonly used in electronic applications to reduce or increase the voltage level in a signal.

3. Phase shifter circuit: The objective is to adjust the phase of the signal arriving at each element of the antenna array, thus modifying the radiation pattern. In the implementation, the JSPHS/2484 component is used as a phase shifter. This device will allow precise control of the phase of the

signal at each antenna in the array. The phase shifters will receive regulated signals from the driver circuit and will adjust their phase according to the established values to achieve the desired directivity.

4. Antenna Patch: the objective is to radiate the adjusted signals with the desired pattern, adapting the system to the operating frequency of WIFI and Bluetooth. For this purpose, a patch antenna array will be used, designed to work in the 2.4 GHz band. The signals whose phase has been adjusted by means of the JSPHS-2484 phase shifters will be fed to the antenna, allowing the radiation pattern to be dynamically modified by varying the phase shifter between the array elements. This array design will be optimized to maximize directivity and minimize losses, ensuring good performance in the wireless applications in which it will be worked.

## B. Signal divider simulation

Fig. 2 shows a 1-to-2 power splitter, which is a passive component used in RF and microwave systems. This type of splitter takes an input signal at port 3 and distributes it into two output signals of equal magnitude at ports 1 and 2. For this research, a Wilkinson splitter was implemented. It is composed of 50-ohms transmission lines (TL13 and TL14) to carry the signal, and an additional transmission line (TL22) helps to achieve the impedance matching and splitting. A 100-ohm resistor (R1) provides isolation between the output ports. When the RF signal enters the TermG connector, it is split into two signals of equal power at the junction of TL13 and TL14. Resistor R1 plays a crucial role by isolating the output ports, preventing interference between the signals and ensuring good signal quality at each port.

Furthermore, the power splitter is designed to maintain 50-ohm impedance for all ports, ensuring efficient power transfer and minimizing signal reflections. The two split signals are delivered through the connectors. This splitter stands out for its good impedance matching, high isolation between ports, and equal power splitting, making it a valuable tool in applications such as wireless communication systems, radars, and measurement equipment.

However, it is important to consider that power splitter has a limited bandwidth and its power is limited by resistance. The simulation of this power splitter was performed in the ADS (Advanced Design System) program, a software widely used in RF and microwave circuit design.

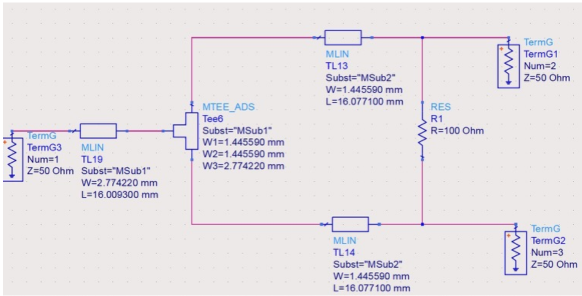


**Fig. 2.** *Power divider simulation*

Fig. 3 shows the frequency response of the Wilkinson power splitter presented before. The blue curve (S1,1) represents the power reflected at the input port (TermG), indicating good impedance matching across the frequency range, as it remains below -20 dB. The red (S1,2) and purple (S1,3) curves represent the power transmitted to the output ports (TermG2 and TermG3), respectively. It is observed that both curves overlap and stay around -3 dB, indicating an equal power split between the two output ports. Furthermore, the flatness of these curves suggests a good performance of the splitter over a wide frequency range. In summary, the graph confirms that the Wilkinson splitter splits the input power equally between the output ports, with good impedance matching and consistent performance over the frequency range analyzed.

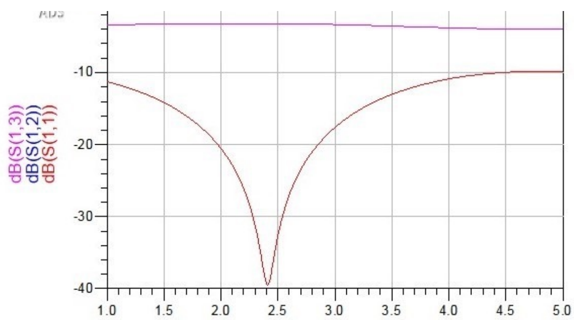


**Fig. 3.** *Power divider radiation pattern*

### C. Simulation of the patch antenna

Fig. 4 shows the design of a rectangular microstrip antenna, modeled on a two-dimensional plane with specific dimensions. The overall width of the design is 66 mm, while its height reaches 61 mm. The design incorporates a 4 mm wide and 36 mm long feed line that connects to the main radiating zone. This radiating zone, with a height of 31 mm, includes cut-out corners, indicating a possible optimization aimed at improving the antenna performance and its adaptation to the intended operating frequency. In addition, the feed port, identified as "Port1", is set as the entry point for the excitation signal. This design seeks to ensure a balance between the antenna's physical dimensions and its electromagnetic performance, meeting coupling and efficiency requirements.

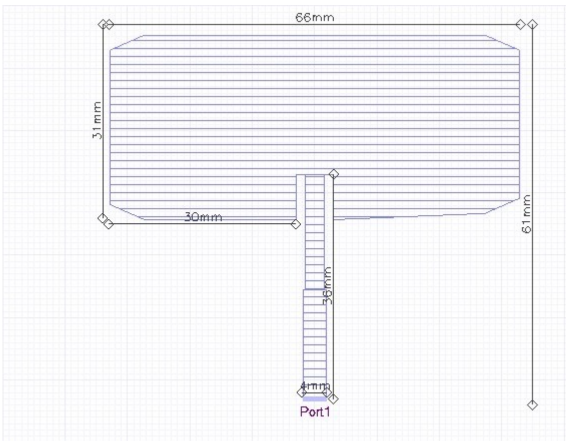


**Fig. 4.** *Patch Antenna*

Fig. 5 shows the magnitude diagram of the reflection coefficient (S11) in dB of an antenna evaluated in the frequency range of 2.00 GHz to 3.00 GHz. This graph was generated by simulation, using specialized software for electromagnetic analysis.

The horizontal axis of the graph shows the frequency in GHz, while the vertical axis shows the reflection coefficient in dB. A value of S11 less than -10 dB indicates that most of the power transmitted from the feed port is radiated by the antenna, representing good performance in impedance matching. The main result shown in this graph reveals that the antenna operates efficiently in a frequency range delimited by the points where S11 crosses the -10 dB threshold. In this case, it is observed that the frequency range is between 2.25 GHz and 2.55 GHz, which determines an operating bandwidth of 300 MHz. This range is suitable for applications that require good radiation in the specified band.

Additionally, the minimum point of the reflection coefficient reaches a value of approximately -42 dB at a frequency of 2.45 GHz, which represents the resonance frequency of the antenna. At this frequency, the power coupling is optimal, maximizing radiation efficiency.

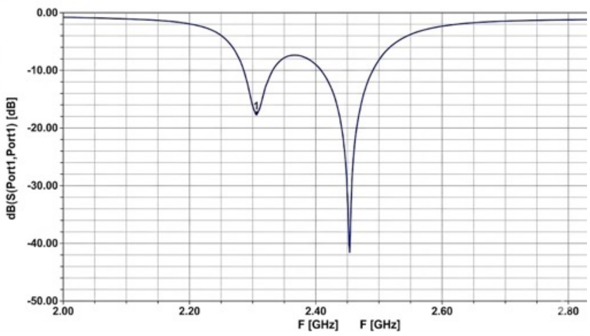


**Fig. 5.** *Reflection coefficient (S11)*

Fig. 6 shows the radiation pattern of the patch antenna operating at 2.4 GHz, a frequency used in WiFi and Bluetooth systems. The horizontal axis represents the Theta angle [°], while the vertical axis shows the magnitude of the electric field in decibels (dB). The graph presents two curves:

• The blue curve: represents the principal component of the electric field, E-theta. A deep "null", i.e., a drastic drop in intensity, is observed at the center of the diagram (0 degrees). This indicates that the antenna does not radiate a signal in that direction.

• The red curve: represents the E-phi component, showing the radiation in a polarization orthogonal to that of the principal component (E-theta). This curve complements the information in the blue curve and helps to understand the antenna's full radiation pattern.

Together, these curves reveal that the patch antenna is directional. Instead of radiating energy evenly in all directions, it concentrates radiation to the sides and forward, with areas of lower radiation in certain directions, such as the center. This directionality is a key feature of antennas designed for applications such as WiFi networks and Bluetooth systems, where efficient coverage is sought towards a specific target area. By concentrating energy in a preferential direction, communication efficiency is improved and interference in other directions is reduced. The radiation pattern shown in the image confirms this directionality, explaining why patch antennas are a common choice in wireless devices that require a defined range and coverage.

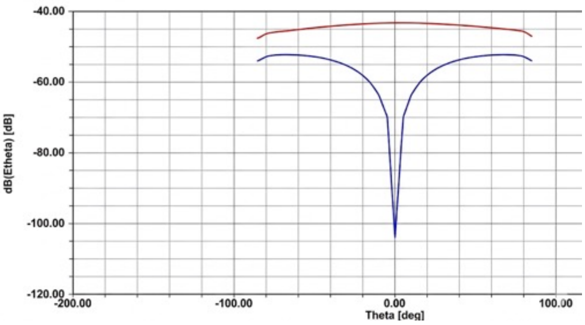


**Fig. 6.** *Radiation pattern (S11) in Ansoft program*

## III. Results

### A. Signal divider implementation

Fig. 7 presents the physical implementation of the microstrip power signal divider, which is a key component in RF and microwave circuits for the 1700/2100 MHz AWS bands. The rectangular shape of the conductive patch and the microstrip lines determine the impedance matching and splitting characteristics. The dielectric material (the yellow part) provides mechanical support and electrical properties for the operation of the divider. The SMA connector allows connection to other circuits or measurement instruments. This divider works by dividing the high frequency current entering through the connector into two equal currents that propagate through the microstrip lines to the outputs. The geometry of the divider is designed to ensure that the power is divided equally and that the impedance is kept matched to avoid signal reflections.

### B. Signal divider implementation

Fig. 7 presents the physical implementation of the microstrip power signal divider, which is a key component in RF and microwave circuits for the 1700/2100 MHz AWS bands. The rectangular shape of the conductive patch and the microstrip lines determine the impedance matching and splitting characteristics. The dielectric material (the yellow part) provides mechanical support and electrical properties for the operation of the divider. The SMA connector allows connection to other circuits or measurement instruments. This divider works by dividing the high

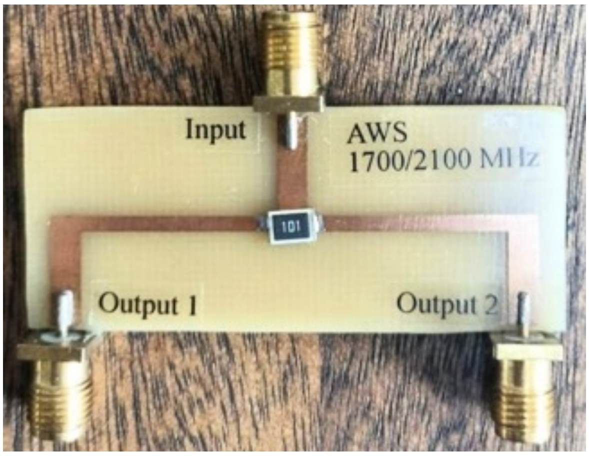


**Fig. 7.** *Physical Implementation of Power Divider*

In addition to its primary function of power splitting, this splitter also plays a crucial role in the realization of antenna arrays. By splitting the input signal and feeding multiple antennas, the splitter allows for the creation of arrays that direct the signal propagation in a specific direction. When designing antenna arrays, splitter characteristics such as power splitting, impedance matching, and isolation between outputs must be carefully considered to achieve the desired radiation pattern and directivity.

### C. Signal divider validation

As a first step to verify the performance of the implemented power splitter, measurements were made with a vector network analyzer (VNA), connecting two 50-ohm coaxial cables to ports 1 and 2 of the divider, while a load resistor at the input as shown in Fig. 8.

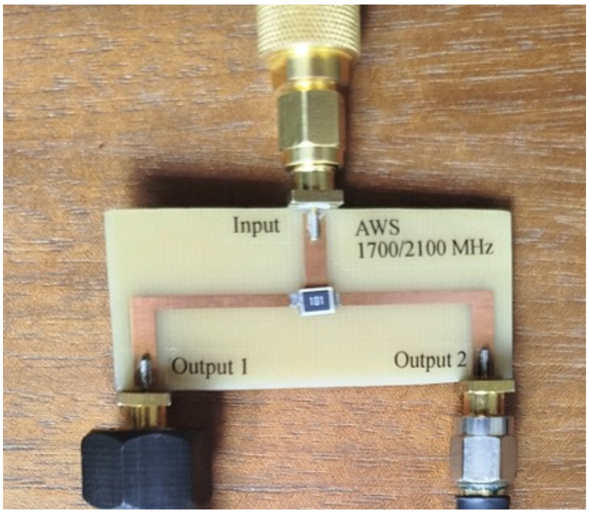


**Fig. 8.** *Power divider with load resistor at input*

Using this configuration, Fig. 9 presents the response of the implemented divider measured using a Vector Network Analyzer (VNA) model E5071C. The main trace represents the reflection coefficient (S11) of the voltage divider as a function of frequency, verified by connecting a load resistor at the divider input. Marker 1 indicates a minimum of -10.135 dB at 2.45 GHz, confirming the correct impedance matching and resonance at this frequency. This result validates the previous simulation in ADS and guarantees efficient filter operation at the desired frequency.

At the same time, Fig. 10 shows the reflection coefficient (S12) of the voltage divider as a function of frequency. For verification, a load resistor was connected to the input of the divider. Marker 1 indicates a minimum of -7.2362 dB at 2.45 GHz, confirming proper impedance and resonance matching at this frequency. This result validates the previous simulation in ADS and ensures efficient filter operation at the desired frequency.

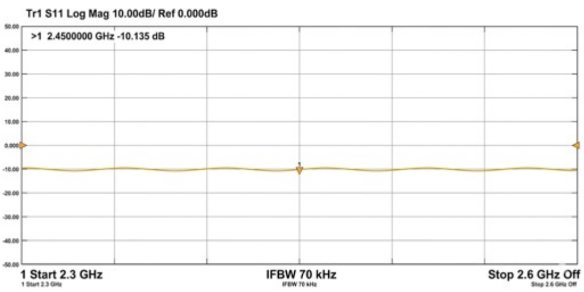


**Fig. 9.** *Reflection coefficient (S11) of the divider input.*

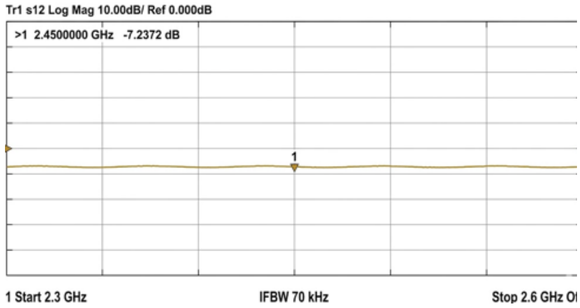


**Fig. 10.** *Reflection coefficient (S12) of the divider input.*

Second step of validation continues with the connections of the splitter as shown in Fig. 11, where the input and output 2 are connected to the VNA, while a 50-ohm load resistor was placed on output 1.

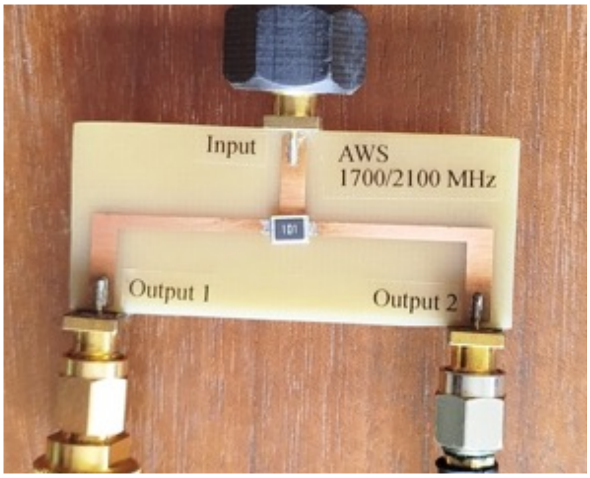


**Fig. 11.** *Power divider with load resistor at output 1*

Under this measurement configuration, Fig. 12 shows the reflection coefficient (S11) of the voltage divider as a function of frequency. Marker 1 indicates a minimum of -7.6613 dB at 2.45 GHz, confirming proper impedance and resonance matching at this frequency. This result validates the previous simulation in ADS and ensures efficient filter operation at the desired frequency.

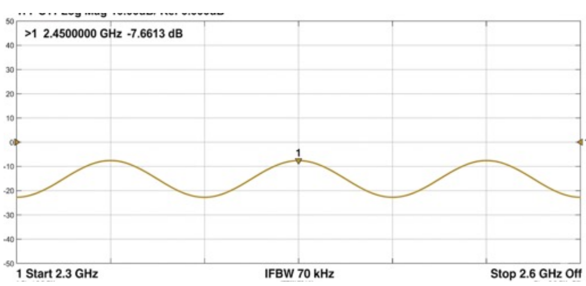


**Fig. 12.** *Reflection coefficient (S11) of output 1 of the divider.*

In addition, Fig. 13 shows the reflection coefficient (S12) of the signal divider as a function of frequency, when a load resistor was connected to output 1 of the divider. Marker 1 indicates a minimum of -5.1342 dB at 2.45 GHz, confirming proper impedance and resonance matching at this frequency. This result validates the previous simulation in ADS and ensures efficient filter operation at the desired frequency.

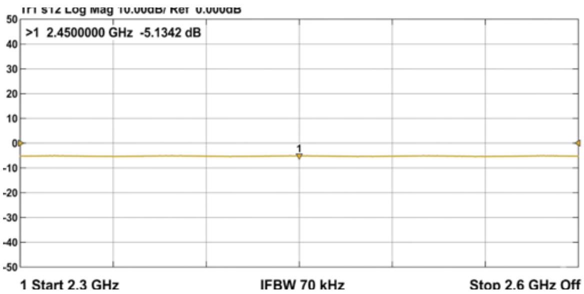


**Fig. 13.** *Reflection coefficient (S11) of output 1 of the divider.*

Third step of validation continues with the connections of the splitter as shown in Fig. 14, where the input and output 1 are connected to the VNA, while a 50-ohm load resistor was placed on output 2.


**Fig. 14.** *Power divider with load resistor at output 2*

Results plotted in Fig. 15 show the reflection coefficient (S11) of the signal divider as a function of frequency. Marker 1 indicates a minimum of -18.018dB at 2.45 GHz, confirming proper impedance and resonance matching at this frequency. This result validates the previous simulation in ADS and ensures efficient filter operation at the desired frequency.

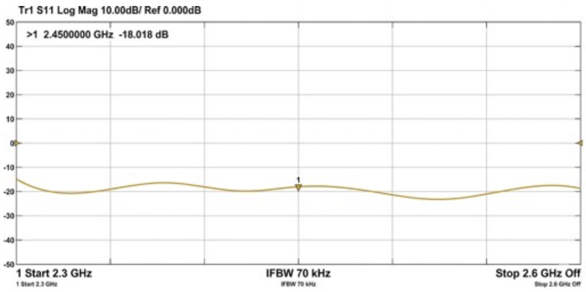


**Fig. 15.** *Reflection coefficient (S11) of output 2 of the divider.*

Also, Fig. 16 shows the reflection coefficient (S12) of the voltage divider as a function of frequency. Marker 1 indicates a minimum of -5.0511 dB at 2.45 GHz, confirming proper impedance and resonance matching at this frequency. This result validates the previous simulation in ADS and ensures efficient filter operation at the desired frequency.

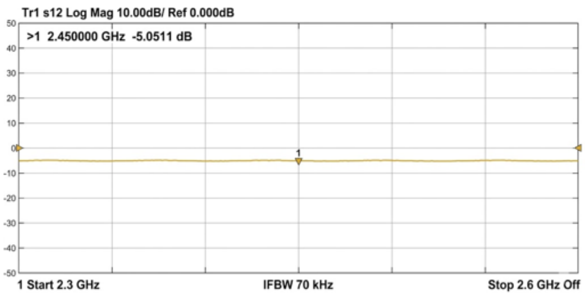


**Fig. 16.** *Reflection coefficient (S12) of output 2 of the divider.*

### D. Implementation of patch antenna

In Fig. 17, the physical implementation of the patch antenna is shown. At this stage, the dimensions and features of the original design are materialized, including the radiating patch, feed line, and signal connector. Manufacturing precision and choice of materials are key factors to ensure that the real antenna reproduces the simulated performance, meeting the stated coupling and efficiency requirements.

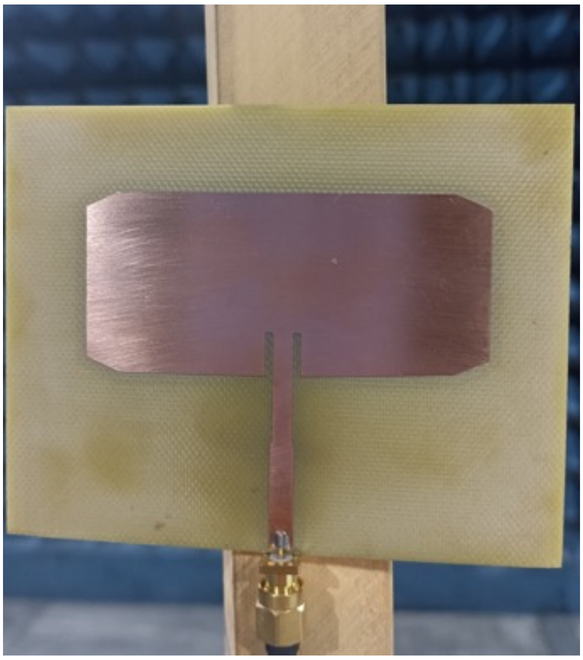

**Fig. 17.** *Physical implementation of Patch Antenna.*

Fig. 18 shows the response of a patch antenna, combining the previous simulation performed in Ansoft with the physical verification of its operation using the VNA. The main trace, “Tr1 S11 Log Mag 10.00dB/ Ref 0.000dB [F1]”, shows the reflection coefficient (S11) of the antenna as a function of frequency. It is observed that marker 3 indicates a minimum of -27.499 dB in S11 at 2.445 GHz, confirming a good impedance and resonance match at this frequency. This result validates the previous simulation in Ansoft and ensures that the antenna operates efficiently at the desired frequency. The graph covers a range from 1 GHz to 5 GHz, with an IFBW (Intermediate Frequency Bandwidth) of 70 kHz and a span of 2 GHz.

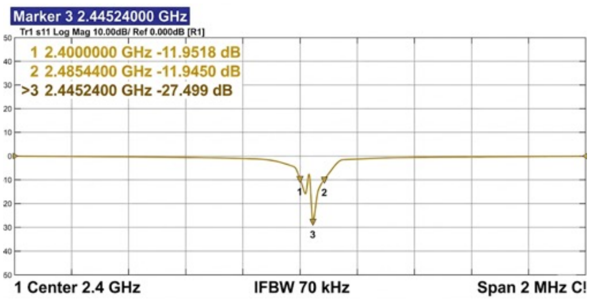


**Fig. 18.** *Patch antenna radiation pattern*

## E. Measurements with antenna array

The initial measurements were made using the antenna matrix as shown in Fig. 19 within an anechoic chamber. To obtain a precise representation of the radiation pattern, measurements were taken every six degrees around 180 degrees, giving a total of 30 measurements to verify the proper operation and observe the highest radiation that occurs in the front of the matrix. The remaining 30 points of the 360 degrees measurements were made later. This methodology allowed a detailed capture of the system response in several directions, facilitating the visualization and analysis of radiation behavior.

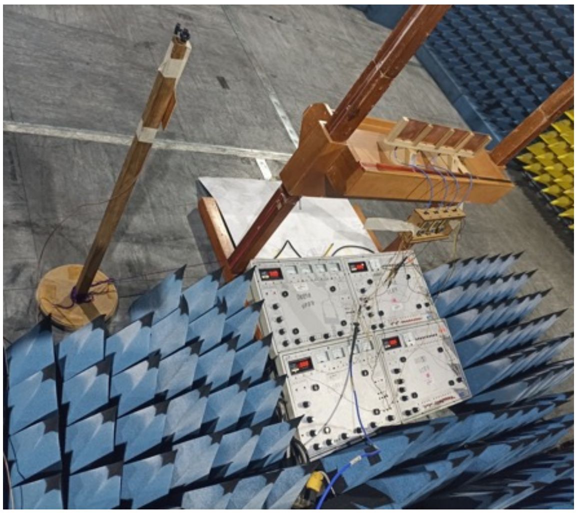

**Fig. 19.** *Antenna arrangement within an anechoic chamber.*

Fig. 20 shows the radiation pattern of the antenna array obtained by measurements at different angles, particularly every 6 degrees. It is observed that the energy is mainly concentrated in one sector of the plane, spanning approximately 0 to 180 degrees on the right side. This radiation pattern confirms that the antenna array is working correctly, since the radiation is not distributed uniformly in all directions, but is concentrated in a specific sector. The shape and direction of the main and secondary lobes, as well as the symmetry of the pattern, are important characteristics that are analyzed to evaluate the performance of the array. In addition, the intensity of the radiation at each angle provides valuable information about the efficiency and directivity of the array.

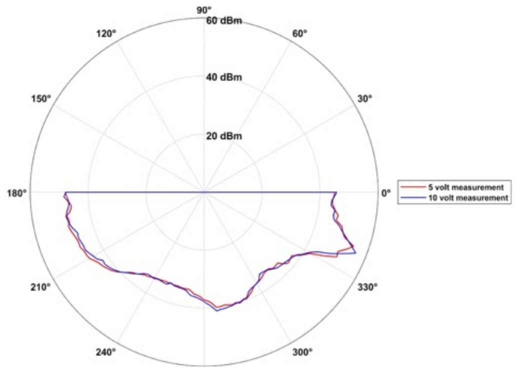


**Fig. 20.** *Radiation pattern of the first measurement in a specific direction.*

The radiation pattern presents two lines: one in blue, corresponding to the measurements made with 10 volts, and another in red, representing the measurements made with 5 volts. This differentiation allows comparing the behavior of the array under different power conditions, which is crucial to evaluate its performance and adaptation to different operating scenarios.

This radiation pattern is critical to determining whether the array meets the requirements of the desired application, such as wireless communications or radar systems. Consequently, this pattern validates the correct implementation of the antenna array and its capability for applications requiring directionality.

### F. Partial measurements for radiation pattern calculation

The measurements were made with an antenna matrix consisting of four patch antennas. For this study, different voltages were assigned to each gear lever to analyze the matrix phase change. During this validation, four voltage sources were used and three different measurements were done. Results obtained are plotted in Fig. 21, where these are compared to the original measurement (blue color), which was acquired without the implementation of the gear lever.

In Fig. 21, the red curve corresponds to a voltage of 3 Volts, where it is observed that there is a phase shift with respect to the original signal. This information allowed a comparison between the radiation diagrams generated with the different voltages applied.

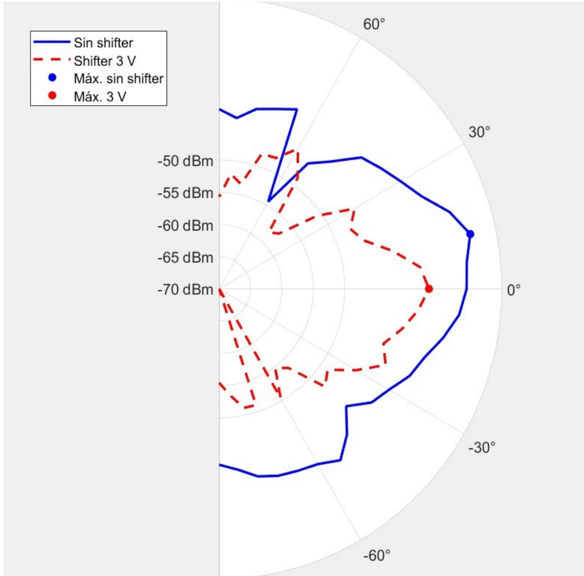


**Fig. 21.** *Radiation Patter at different voltage in the "shifter".*

When performing the comparative analysis between the measurements with variation in the gear levers and the original measurement, it is observed that the original measurement has a greater power compared to the measurements with variation. This is due to the dispersion losses caused by the connectors, cables and gear levers, which generate a phase shift in the matrix, but with a significant attenuation of the signal

### G. Linear measurement every 10 cm

Fig. 22 shows a linear measurement performed with an antenna array. To perform this measurement, values were recorded over a distance extending from the center point to 110 centimeters, with a variation of 10 centimeters per point. This measurement was performed in both directions, i.e., from the center toward the positive (right) and negative (left) side of the central reference.

This process allowed obtaining a detailed representation of the distribution of the signal or property measured in a symmetrical range around the center of the antenna array configuration. Taking data in both directions facilitates a more complete analysis of the signal propagation or behavior as a function of distance from the source, which is essential for evaluating characteristics such as directivity, coverage, or uniformity of the antenna system.

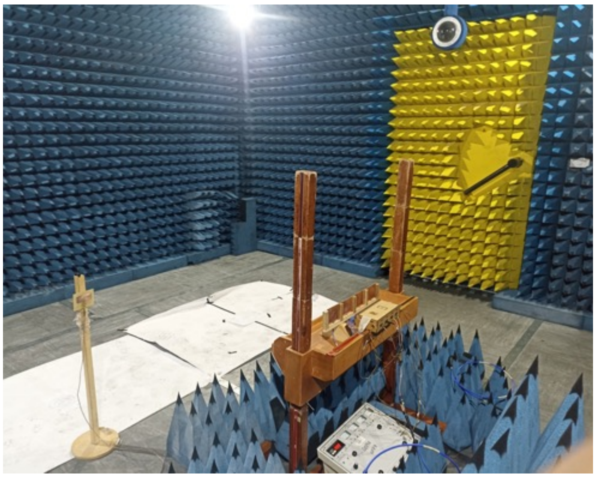

**Fig. 22.** *Linear measurement with an antenna array within an anechoic chamber.*

The radiation pattern obtained from measurements made with the antenna array in a linear configuration, spanning from 0 to 110 centimeters in both the positive and negative directions, is shown in Fig. 23. These measurements were made at 3 volts and without a shifter, which allowed a detailed phase shift of 12 degrees to be observed in the signals. The blue curve represents the reference, that is, the measurements made without the use of a phase shifter. The red curve represents the signal generated from 3 volts.

This graph clearly visualizes the behavior of the antenna array under different power conditions. A constant angular shift of the radiation pattern is observed in the curve where a voltage was applied, compared to the reference curve.

Specifically, a phase shift of approximately 12 degrees is identified in the curves corresponding to the different voltage levels with respect to the curve without a shifter, confirming the expected effect of phase control on the main lobe direction.

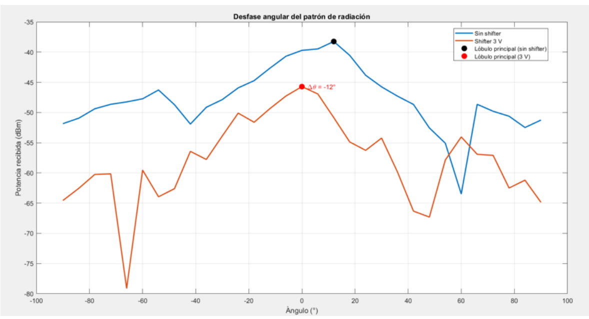


**Fig. 23.** *Linear measurement with an antenna array.*

## V. Conclusions

The measurements were made in an anechoic chamber, which allowed to register radiation patterns with high precision, eliminating external reflections that could interfere with the real characterization of the antenna arrangement. This methodology guarantees The measurements were made in an anechoic chamber, which allowed to register radiation patterns with high precision, eliminating external reflections that could interfere with the real characterization of the antenna arrangement. This methodology guarantees that the results obtained are representative of the electromagnetic behavior of the system in controlled conditions. An angular shift of approximately 12 degrees was observed in the radiation pattern when different voltage levels (3V, 6V, 9V, 12V, and 15V) were applied to the phase shifters, compared to the reference curve without a phase shifter. This result validates the correct operation of the phase control system and its ability to steer the main lobe of the beam in a specific direction. The system proved effective for adaptive wireless communications applications, allowing dynamic modification of the antenna array's radiation pattern. This feature is especially useful in environments such as smart homes or IoT devices, where signal targeting is required to improve coverage and reduce interference.

## VI. References

[1] C. Systems, "WiFi technology overview," Tech. Rep., 2016. [Online]. Available: https://www.cisco.com

[2] D. M. Pozar, Microwave Engineering, 3rd ed. Wiley, 2005.

[3] C. A. Balanis, "Antenna theory: Analysis and design," 2016.

[4] G. V. Tsoulos, Adaptive Antennas for Wireless Communications. Wiley, 2001.

[5] M. A. Hossain and M. T. Islam, "Compact and high-performance microstrip patch antennas for IoT applications," Sensors, vol. 20, no. 8, p. 2272, 2020.

[6] T. Lim, S. Gao, and T. Loh, "Design of beam-steering microstrip array antennas using

phase shifters," IEEE Transactions on Antennas and Propagation, vol. 63, no. 7, pp. 3079–3086, 2015.

[7] I. S. Association, IEEE 802.11ax: High-Efficiency WLAN, Std., 2021.

[8] P. Goel and K. J. Vinoy, "A low-cost phased array antenna integrated with phase shifters," Progress In Electromagnetics Research B, vol. 30, pp. 255–277, 2011.

[9] A. Karmakar, B. Roy, and A. K. Bhattacharjee, "Mems- based monolithic phased array using 3-bit switched-line phase shifter," Advanced Electromagnetics, 2025. [Online]. Available: https://aemjournal.org/index.php/AEM/article/view/520

[10] C. Paz, "Diseño y simulación de un sistema radiante basado en antenas yagi-uda que implemente la técnica de beamforming a una frecuencia de operación de 6 GHz," Master's thesis, Repositorio EPN, 2022, s.l.

[11] M. Amri and F. Echouchene, "Phased array antenna structure based on novel 6-bit phase shifter for WiFi communication systems," International Review of Electrical and Computer Engineering, vol. 15, no. 1, pp. 10– 18, 2025.